

MedLoRD: A Medical Low-Resource Diffusion Model for High-Resolution 3D CT Image Synthesis

Marvin Seyfarth^{1,4}, Salman Ul Hassan Dar^{1,2,3,4}, Isabelle Ayx⁵, Matthias Alexander Fink⁶, Stefan O. Schoenberg^{2,5}, Hans-Ulrich Kauczor⁶, and Sandy Engelhardt^{1,2,4}

¹ Department of Internal Medicine III, Heidelberg University Hospital, Germany

² AI Health Innovation Cluster (AIH), Germany

³ Heidelberg Faculty of Medicine, Heidelberg University, Germany

⁴ German Centre for Cardiovascular Research (DZHK), Partner site Heidelberg/Mannheim, Germany

⁵ Department of Radiology and Nuclear Medicine, University Medical Center Mannheim, Germany

⁶ Clinic for Diagnostic and Interventional Radiology, Heidelberg University Hospital, Heidelberg, Germany

Marvin.Seyfarth@med.uni-heidelberg.de

Abstract. Advancements in AI for medical imaging offer significant potential. However, their applications are constrained by the limited availability of data and the reluctance of medical centers to share it due to patient privacy concerns. Generative models present a promising solution by creating synthetic data as a substitute for real patient data. However, medical images are typically high-dimensional, and current state-of-the-art methods are often impractical for computational resource-constrained healthcare environments. These models rely on data sub-sampling, raising doubts about their feasibility and real-world applicability. Furthermore, many of these models are evaluated on quantitative metrics that alone can be misleading in assessing the image quality and clinical meaningfulness of the generated images. To address this, we introduce MedLoRD, a generative diffusion model designed for computational resource-constrained environments. MedLoRD is capable of generating high-dimensional medical volumes with resolutions up to $512 \times 512 \times 256$, utilizing GPUs with only 24GB VRAM, which are commonly found in standard desktop workstations. MedLoRD is evaluated across multiple modalities, including Coronary Computed Tomography Angiography and Lung Computed Tomography datasets. Extensive evaluations through radiological evaluation, relative regional volume analysis, adherence to conditional masks, and downstream tasks show that MedLoRD generates high-fidelity images closely adhering to segmentation mask conditions, surpassing the capabilities of current state-of-the-art generative models for medical image synthesis in computational resource-constrained environments.

Keywords: Generative AI · Resource constrained · Image evaluation.

1 Introduction

Generative AI has emerged as a promising solution for models to learn data distributions and generate synthetic samples that can expand datasets or serve as privacy-preserving substitutes for real patient data [8,15].

Despite progress, challenges remain in real-world implementation. Medical imaging data is high-dimensional, making it difficult for generative models to operate efficiently with limited GPU resources. Some approaches downsample data to capture global structures [19,11,3] but risk losing fine-grained details critical for diagnosis, while others apply post-processing techniques [5] that may introduce artifacts. Additionally, many studies rely on high-end GPUs that are often unavailable in clinical environments, creating a gap between research and practical implementation [5,18]. Even when computational resources are available, evaluating generative models remains challenging. Standard metrics like Fréchet Inception Distance (FID) [6], while widely used in computer vision, often fail to capture clinically relevant details, making it difficult to assess the true diagnostic utility of synthetic images [17].

To address these challenges, we introduce MedLoRD, a Medical Low Resource latent Diffusion model for medical image synthesis. MedLoRD uses VQ-VAE GANs for encoding and a 3D UNet for image denoising in the latent space. With efficient architectures and optimized code, it generates high-quality volumetric images up to $512 \times 512 \times 256$ on GPUs with 24GB VRAM, without post-processing. It also works effectively in conditional settings. To assess the model’s clinical relevance, we conduct extensive evaluations, including radiological assessment, regional volume analysis, quantitative metrics such as FID and DICE, as well as performance testing on downstream tasks. Our results show that MedLoRD generates diagnostically useful images while operating within practical computational constraints, bringing us closer to real-world deployment in medical imaging.

2 Methodology

MedLoRD is based on the concept of latent diffusion models [12]. In this study, we deploy a Vector Quantised Variational Autoencoder (VQ-VAE) with perceptual and adversarial loss as a first-stage compression network to project images into a latent space. Noise is then added to the latent representation over T timesteps. A U-Net is subsequently trained in the latent space to predict a combination of noise and the input sample [12]. To process 3D volumes, 2D convolutions are replaced with 3D convolutions. For the conditional generative model, a ControlNet is applied [20], where each condition is processed in a separate input channel. Typically, ControlNet is initialized as a copy of the encoder and middle blocks of the pretrained unconditional model. In contrast, we initialized it with 50% fewer channels and train it from scratch. This approach enables efficient control while reducing memory usage. Models were implemented using the MONAI library [1] and code is heavily inspired by <https://github.com/Warvito/monai-vqvae-diffusion/tree/main>

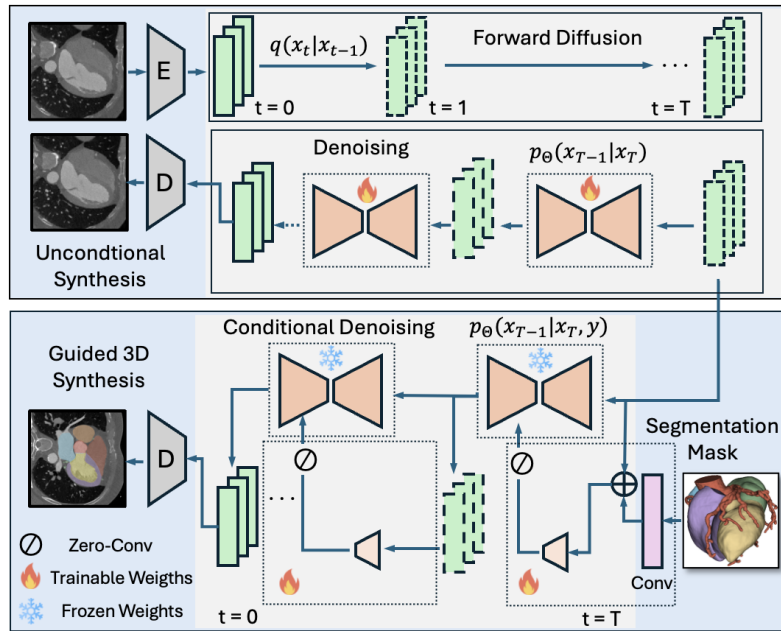


Fig. 1. Top: A 3D U-Net is trained in the latent space of an autoencoder. Bottom: A ControlNet with 50% reduced size is trained from scratch to incorporate conditions.

and <https://github.com/Project-MONAI/GenerativeModels>. The implementation, along with configuration files, are publicly available at: <https://github.com/Cardio-AI/medlord>

2.1 Datasets

Photon Counting Coronary Computed Tomography Angiography (PC-CTA): This dataset consisted of 136 CCTA volumes (3D) acquired at the University Medical Centre Mannheim, with ethics approval granted by the Ethics Committee of Ethikkommission II at Heidelberg University (ID 2021-659). Among these, 120 volumes were reserved for training and 16 for testing. All volumes were center-cropped to a size of $512 \times 512 \times 256$, and intensity-clipped between -1000 and 2000. **Lung CT (LUNA):** This dataset comprised of 888 lung volumes (3D) from the publicly available Luna16 dataset [13]. Among these, 800 volumes were used for training, and 88 volumes for testing. The volumes were resized to $512 \times 512 \times 256$, and intensity-clipped between -1000 and 2000.

2.2 Competing Methods

MAISI: MAISI is built on latent diffusion models, utilizing a variational autoencoder GAN to encode data [5]. The diffusion model is also conditioned on

the voxel spacing of the volumes. During synthesis, to manage computational constraints, decoding is performed on 3D patches in the latent space, followed by volume-stitching to reconstruct complete volumes. Training procedures, hyperparameters, and pre-trained foundation autoencoder were adapted from <https://github.com/Project-MONAI/tutorials/tree/main/generation/maisi>. For model training, all data samples were downsampled to $512 \times 512 \times 128$ to fit within the available GPU VRAM, as measured GPU memory consumption did not align with the reported values in the repository. This discrepancy may be due to differences in GPU architecture, as the original implementation used A100/V100 GPUs, which are optimized for performance and may handle memory allocation differently, and further did not account for encoding/decoding steps. Two variants of MAISI were considered. In the first variant, MAISI_{ST}, the encoding model was trained from scratch, and in the second variant, MAISI_{PT}, a pre-trained foundation encoding model trained on around 40k CT images was adapted. In the PCCTA dataset, MedLoRD was compared to both MAISI_{ST} and MAISI_{PT}, whereas in the LUNA dataset, only the better-performing MAISI variant (MAISI_{PT}) was used due to extensive training times.

VQ-Trans: VQ-Trans combines VQVAE-GAN and transformers [4]. First, a VQVAE-GAN is trained to encode the image into a latent space. Then, a transformer is trained to sequentially predict voxels in the latent space, starting from the first randomly initialized voxel. Upon sampling in the latent space, a decoder is used to decode the image back into the pixel space. The encoding model was utilized to down-sample the data by 16 to have a sequence length of 12544.

HA-GAN: HA-GAN is a GAN-based model that integrates adversarial loss with an additional reconstruction loss for improved performance [14]. All training procedures and hyperparameters were adapted from <https://github.com/batmanlab/HA-GAN>.

2.3 Training Details

MedLoRD’s autoencoders were trained on patches of size $128 \times 128 \times 128$ for the PCCTA dataset and $128 \times 128 \times 64$ for the LUNA dataset, cropped at randomly sampled centers of the original images, for 250,000 iterations. The best-performing epoch was selected based on MS-SSIM, PSNR, and perceptual LPIPS loss values calculated on the held-out test samples. The number of training iterations was adopted from the respective repository if reported; otherwise, generative models were trained for 750,000 iterations, with the best-performing epoch chosen based on the lowest FID score and visual evaluation. For each evaluation interval, we synthesized 120 samples for PCCTA and 88 samples for LUNA. In MedLoRD, a cosine noise schedule [10] with $T=300$ timesteps was used for training diffusion models, and L1-loss was minimized using the AdamW optimizer [9]. All experiments, including model training, inference, and evaluation, were designed to be conducted on a single RTX 3090 24 GB GPU with CUDA 12.2.

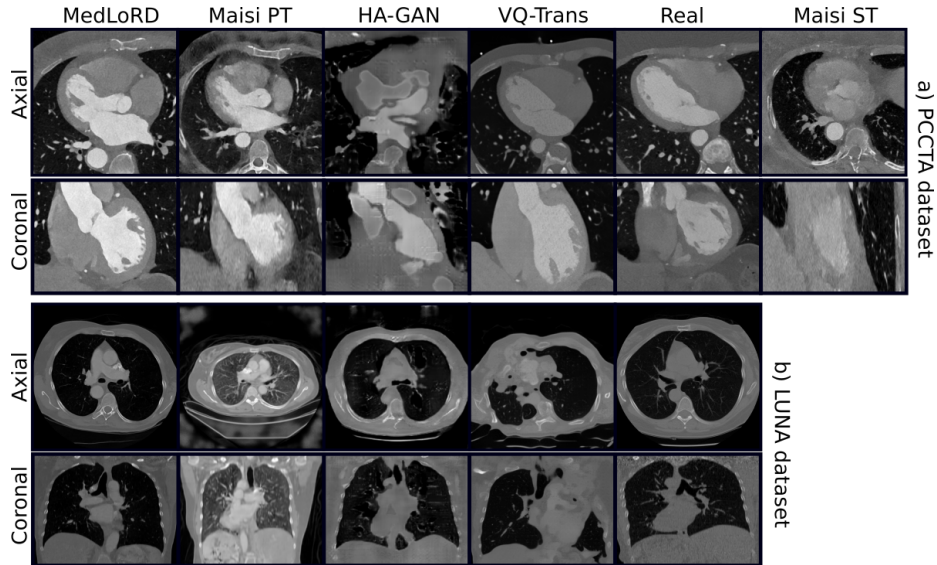


Fig. 2. Randomly selected unconditional samples for each method. Additional MedLoRD samples are provided in the supplementary material.

3 Results

3.1 Unconditional Synthesis

First, we conducted unconditional image synthesis, and Fig. 2 presents representative samples from both the PCCTA and LUNA datasets. MedLoRD consistently generates high-quality, realistic images, preserving both global and local structural details. In contrast, other models exhibited unstable behavior, with some samples showing poor quality and heavy artifacts. VQ-Trans produced reasonable images but exhibited some loss of fine structural details and the presence of artifacts. HA-GAN, on the other hand, failed to generate realistic images. MAISI_{ST} generated images where the global structure was mostly recovered; however, heart structures were completely lost. Using MAISI’s pre-trained foundation encoding model (MAISI_{PT}) significantly improved sample quality, although synthetic images still contained clear artifacts and distortions in the PCCTA dataset.

To quantitatively assess the generated samples, a commonly used metric FID was computed between testing and synthetic images generated by each method.

Table 1. FID Scores for Different Methods on Luna and PCCTA Datasets

Dataset	MedLoRD	MAISI _{ST}	MAISI _{PT}	HA-GAN	VQ-Trans	Real
PCCTA	0.0188	0.09	0.032	0.03373	0.022	29
Luna	0.008	-	0.019	0.003	0.012	0.0053

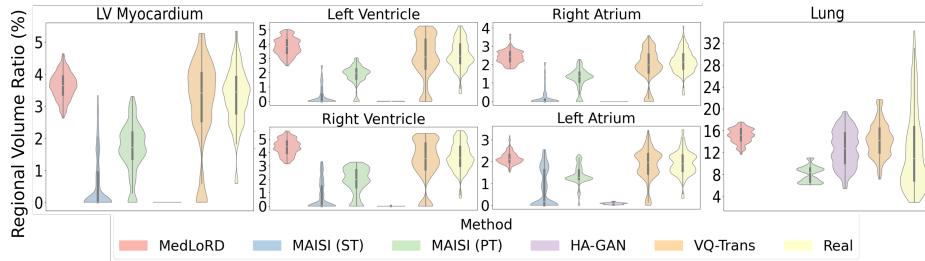


Fig. 3. Regional volume ratio distributions for the PCCTA dataset (left ventricle myocardium, aorta, ventricles, atria, pulmonary artery) and lung dataset.

For reference, we also calculated FID between testing and training samples. The results, summarized in Table 1, reveal inconsistencies between FID scores and actual image quality. In the PCCTA dataset, real samples had the highest FID, contradicting expectations. In the LUNA dataset, HA-GAN—despite producing unrealistic images—had the lowest FID. These results suggest that FID alone is an unreliable metric for evaluating medical image synthesis, as it does not always align with visual assessments, especially in small datasets.

To provide a more comprehensive evaluation, we included an additional quality metric, the Regional Volume Ratio (RVR). The RVR is calculated by dividing the number of voxels within the masked region of interest by the total number of voxels, assessing whether the generated volumes of regions align with real volume distributions. Segmentation masks for various regions in the PCCTA and LUNA datasets were obtained using TotalSegmentator [16]. These values were then compared to the corresponding values from real images, as provided by the training samples for each dataset. To remove extreme outliers, we truncated the acquired distributions to include only values between the 1st and 99th percentile. Fig.3 illustrates these comparisons, showing that MedLoRD-generated images exhibited structural distributions most closely aligned with real samples. A key observation is that while the distributions in MedLoRD-generated images fall within the real range, they exhibit lower variance. This might be explained by using L1 loss for training, converging more towards the median distributions. Given the limitations of traditional metrics, we conducted a radiological evaluation to assess the clinical quality of the generated images, with each dataset evaluated by a corresponding expert, following the criteria outlined in Fig. 4. Fig. 4 presents the radiological assessments. In the PCCTA dataset, MedLoRD outperforms all competing methods, with 6/10 synthesized samples indistinguishable from real ones, showcasing its strong generative capabilities. In the LUNA dataset, MedLoRD performs competitively, with only MAISI_{PT} achieving higher radiological interest. However, 96% of the 40k CT images used to pre-train MAISI_{PT}’s encoding model were chest scans, potentially giving it an advantage in lung image synthesis, due to a more comprehensive latent space. MedLoRD still outperforms all other competing methods. Taken together these

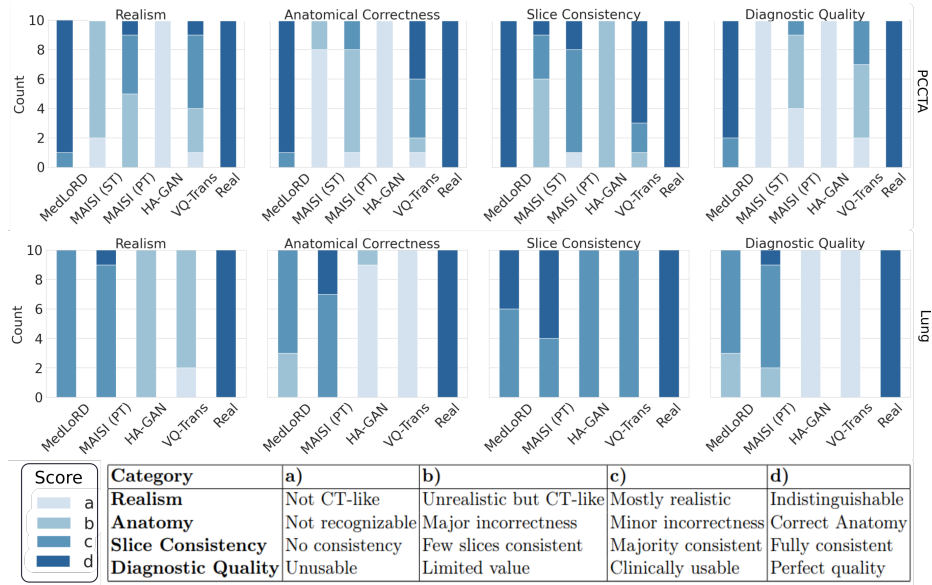


Fig. 4. Radiological evaluation. Top: PCCTA dataset. Bottom: Lung dataset. Images were randomly selected and then shuffled across methods ensuring blinded assessment.

results suggest that MedLoRD is able to achieve state of the art performance compared to the competing methods.

3.2 Conditional Synthesis

We also evaluated MedLoRD’s ability to synthesize samples based on spatial conditions by generating volumes from input conditional masks, which were taken from the held-out test set and were never seen during the training of either the unconditional or conditional models. We then extracted masks from the synthesized images using TotalSegmentator and compared them to the input masks. Tab. 2 shows the corresponding DICE scores (DSC). High DSC for multiple regions indicates that MedLoRD synthesizes volumes consistent with the input masks in both the PCCTA and LUNA datasets. Notably, regions with contrast agent, such as the aorta, left atrium (LA) and left ventricle (LV), exhibited higher DICE scores compared to regions without contrast agent. This difference could stem from the limited accuracy of TotalSegmentator in segmenting these regions, as contrast-enhanced areas tend to have more clearly defined boundaries. Additionally, no data augmentation was applied, which may explain the observed performance gap, as augmentation could potentially improve generalization, especially in smaller datasets like PCCTA. Fig. 5 also shows some representative samples adhering to their input segmentation masks.

Finally, we evaluated the model on downstream tasks: segmenting the LV myocardium and left ventricle in PCCTA, and segmenting the lungs in LUNA using

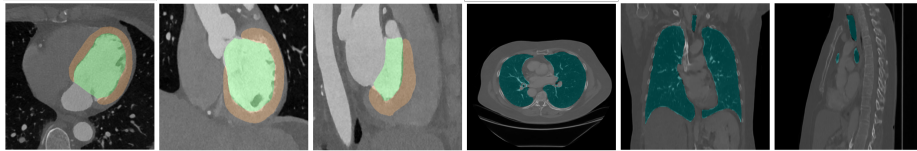


Fig. 5. Conditional samples. Highlighted in color are input condition masks. Green: Left ventricle (LV), Orange: LV Myocardium, Cyan: Lung

nnUNet [7]. We compared models trained on all real data versus those trained on an equal number of synthetic data. The results suggest that replacing real data with synthetic data had minimal impact on downstream performance.

4 Discussion

We introduced a low-resource diffusion model trained on volumes of size $512 \times 512 \times 256$, capable of synthesizing high-resolution images on a GPU with 24GB VRAM—hardware commonly found in many desktop setups. Extensive evaluations on the PCCTA dataset demonstrated outstanding performance in traditional metrics, as well as generating structures according to real volume distributions. Additionally, our model excelled in radiological evaluation, even when compared to a state-of-the-art generative model with a foundational encoder, MAISI_{PT}. To further assess its performance, we evaluated our model on a lung dataset, where MAISI_{PT}’s encoder had undergone extensive training. While our model outperformed competing methods like HA-GAN and VQ-Trans in traditional metrics, radiological evaluation revealed that, although superior to these methods, its synthetic samples exhibited less radiological value compared to those generated by MAISI_{PT}. This may be due to differences in the underlying training conditions, which led to more detailed representations of radiologically important regions in MAISI_{PT}. There has been limited effort in thoroughly evaluating the quality and diagnostic reliability of synthesized images, a gap our work aims to address. Our evaluation methods provide a more comprehensive assessment than those used in previous studies, covering multiple aspects of image quality. Our results highlight that relying on a single metric can lead to misleading conclusions. In the future, we also plan to integrate additional evaluation factors into the model training pipeline, such as data memorization [2]. Lastly,

Table 2. Medians and IQRs of DICE for different input conditions and downstream task (DT) performance on held-out test samples.

Metric	Aorta	LA	RA	LV Myo	LV	RV	Lung
DICE	0.87(0.09)	0.85(0.11)	0.81(0.09)	0.73(0.15)	0.89(0.13)	0.80(0.08)	0.98(0.00)
DICE DT real	-	-	-	0.97(0.01)	0.98(0.01)	-	0.99(0.00)
DICE DT syn	-	-	-	0.92(0.03)	0.96(0.03)	-	0.98(0.01)

we evaluated our model in a conditional setting and found that replacing real data with synthetic data had no significant impact on downstream tasks across both datasets, reinforcing the value of our model’s synthesized samples.

Acknowledgments. This work was supported through state funds approved by the State Parliament of Baden-Württemberg for the Innovation Campus Health + Life Science Alliance Heidelberg Mannheim, Heidelberg Faculty of Medicine at Heidelberg University, BMBF-SWAG Project 01KD2215D, and by the Multi-DimensionAI project of the Carl Zeiss Foundation (P2022-08-010). The authors acknowledge **1-** the data storage service SDS@hd supported by the Ministry of Science, Research and the Arts Baden-Württemberg (MWK) and the German Research Foundation (DFG) through grant INST 35/1314-1 FUGG and INST 35/1503-1 FUGG, **2-** the state of Baden-Württemberg through bwHPC and the German Research Foundation (DFG) through grant INST 35/1597-1 FUGG.

References

1. Cardoso, M.J., Li, W., Brown, R., Ma, N., Kerfoot, E., Wang, Y., Murrey, B., Myronenko, A., Zhao, C., Yang, D., Nath, V., He, Y., Xu, Z., Hatamizadeh, A., Myronenko, A., Zhu, W., Liu, Y., Zheng, M., Tang, Y., Yang, I., Zephyr, M., Hashemian, B., Alle, S., Darestani, M.Z., Budd, C., Modat, M., Vercauteren, T., Wang, G., Li, Y., Hu, Y., Fu, Y., Gorman, B., Johnson, H., Genereaux, B., Erdal, B.S., Gupta, V., Diaz-Pinto, A., Dourson, A., Maier-Hein, L., Jaeger, P.F., Baumgartner, M., Kalpathy-Cramer, J., Flores, M., Kirby, J., Cooper, L.A.D., Roth, H.R., Xu, D., Bericat, D., Floca, R., Zhou, S.K., Shuaib, H., Farahani, K., Maier-Hein, K.H., Aylward, S., Dogra, P., Ourselin, S., Feng, A.: Monai: An open-source framework for deep learning in healthcare (2022), <https://arxiv.org/abs/2211.02701>
2. Dar, S.U.H., Seyfarth, M., Ayx, I., Papavassiliu, T., Schoenberg, S.O., Siepmann, R.M., Laqua, F.C., Kahmann, J., Frey, N., Baeßler, B., Foersch, S., Truhn, D., Kather, J.N., Engelhardt, S.: Unconditional latent diffusion models memorize patient imaging data: Implications for openly sharing synthetic data (2025), <https://arxiv.org/abs/2402.01054>
3. Dorjsembe, Z., Pao, H.K., Odonchimed, S., Xiao, F.: Conditional diffusion models for semantic 3d brain mri synthesis. *IEEE Journal of Biomedical and Health Informatics* (2024). <https://doi.org/10.1109/JBHI.2024.3385504>
4. Graham, M.S., Tudosiu, P.D., Wright, P., Pinaya, W.H.L., Jean-Marie, U., Mah, Y.H., Teo, J.T., Jager, R., Werring, D., Nachev, P., et al.: Transformer-based out-of-distribution detection for clinically safe segmentation. In: *International Conference on Medical Imaging with Deep Learning*, pp. 457–476. PMLR (2022)
5. Guo, P., Zhao, C., Yang, D., Xu, Z., Nath, V., Tang, Y., Simon, B., Belue, M., Harmon, S., Turkbey, B., Xu, D.: Maisi: Medical ai for synthetic imaging. In: *Proceedings of the Winter Conference on Applications of Computer Vision (WACV)*, pp. 4430–4441 (February 2025)
6. Heusel, M., Ramsauer, H., Unterthiner, T., Nessler, B., Hochreiter, S.: Gans trained by a two time-scale update rule converge to a local nash equilibrium. In: Guyon, I., Luxburg, U.V., Bengio, S., Wallach, H., Fergus, R., Vishwanathan, S., Garnett, R. (eds.) *Advances in Neural Information Processing Systems*. vol. 30. Curran

- Associates, Inc. (2017), https://proceedings.neurips.cc/paper_files/paper/2017/file/8a1d694707eb0fefe65871369074926d-Paper.pdf
7. Isensee, F., Jaeger, P.F., Kohl, S.A., Petersen, J., Maier-Hein, K.H.: nnu-net: a self-configuring method for deep learning-based biomedical image segmentation. *Nature methods* **18**(2), 203–211 (2021)
 8. Khader, F., Müller-Franzes, G., Tayebi Arasteh, S., Han, T., Haarbuerger, C., Schulze-Hagen, M., Schad, P., Engelhardt, S., Baeßler, B., Foersch, S., Stegmaier, J., Kuhl, C., Nebelung, S., Kather, J.N., Truhn, D.: Denoising diffusion probabilistic models for 3D medical image generation. *Scientific Reports* **13**(1), 7303 (2023). <https://doi.org/10.1038/s41598-023-34341-2>
 9. Loshchilov, I., Hutter, F.: Decoupled weight decay regularization. In: International Conference on Learning Representations (2019), <https://openreview.net/forum?id=Bkg6RiCqY7>
 10. Nichol, A.Q., Dhariwal, P.: Improved denoising diffusion probabilistic models. In: Meila, M., Zhang, T. (eds.) *Proceedings of the 38th International Conference on Machine Learning*. *Proceedings of Machine Learning Research*, vol. 139, pp. 8162–8171. PMLR (18–24 Jul 2021), <https://proceedings.mlr.press/v139/nichol21a.html>
 11. Peng, W., Adeli, E., Bosschieter, T., Park, S.H., Zhao, Q., Pohl, K.M.: Generating realistic brain mris via a conditional diffusion probabilistic model. In: *Medical Image Computing and Computer Assisted Intervention – MICCAI 2023*. p. 14–24. Springer-Verlag, Berlin, Heidelberg (2023). https://doi.org/10.1007/978-3-031-43993-3_2, https://doi.org/10.1007/978-3-031-43993-3_2
 12. Rombach, R., Blattmann, A., Lorenz, D., Esser, P., Ommer, B.: High-resolution image synthesis with latent diffusion models (2021)
 13. Setio, A.A.A., Traverso, A., de Bel, T., Berens, M.S., van den Bogaard, C., Cerello, P., Chen, H., Dou, Q., Fantacci, M.E., Geurts, B., van der Gugten, R., Heng, P.A., Jansen, B., de Kaste, M.M., Kotov, V., Lin, J.Y.H., Manders, J.T., Sónora-Mengana, A., García-Naranjo, J.C., Papavasileiou, E., Prokop, M., Saletta, M., Schaefer-Prokop, C.M., Scholten, E.T., Scholten, L., Snoeren, M.M., Torres, E.L., Vandemeulebroucke, J., Walasek, N., Zuidhof, G.C., van Ginneken, B., Jacobs, C.: Validation, comparison, and combination of algorithms for automatic detection of pulmonary nodules in computed tomography images: The luna16 challenge. *Medical Image Analysis* **42**, 1–13 (2017). <https://doi.org/https://doi.org/10.1016/j.media.2017.06.015>, <https://www.sciencedirect.com/science/article/pii/S1361841517301020>
 14. Sun, L., Chen, J., Xu, Y., Gong, M., Yu, K., Batmanghelich, K.: Hierarchical amortized gan for 3d high resolution medical image synthesis. *IEEE Journal of Biomedical and Health Informatics* **26**(8), 3966–3975 (2022). <https://doi.org/10.1109/JBHI.2022.3172976>
 15. Tudosiu, P.D., Pinaya, W.H., Ferreira Da Costa, P., Dafflon, J., Patel, A., Borges, P., Fernandez, V., Graham, M.S., Gray, R.J., Nachev, P., et al.: Realistic morphology-preserving generative modelling of the brain. *Nature Machine Intelligence* pp. 1–9 (2024). <https://doi.org/10.1038/s42256-024-00864-0>
 16. Wasserthal, J., Breit, H.C., Meyer, M.T., Pradella, M., Hinck, D., Sauter, A.W., Heye, T., Boll, D.T., Cyriac, J., Yang, S., Bach, M., Segeroth, M.: Totalsegmentator: Robust segmentation of 104 anatomic structures in ct images. *Radiology: Artificial Intelligence* **5**(5), e230024 (2023). <https://doi.org/10.1148/ryai.230024>, <https://doi.org/10.1148/ryai.230024>

17. Woodland, M., Castelo, A., Al Taie, M., Albuquerque Marques Silva, J., Eltaher, M., Mohn, F., Shieh, A., Kundu, S., Yung, J.P., Patel, A.B., Brock, K.K.: Feature extraction for generative medical imaging evaluation: New evidence against an evolving trend. In: Linguraru, M.G., Dou, Q., Feragen, A., Giannarou, S., Glocker, B., Lekadir, K., Schnabel, J.A. (eds.) *Medical Image Computing and Computer Assisted Intervention – MICCAI 2024*. pp. 87–97. Springer Nature Switzerland, Cham (2024)
18. Xu, Y., Sun, L., Peng, W., Jia, S., Morrison, K., Perer, A., Zandifar, A., Visweswaran, S., Eslami, M., Batmanghelich, K.: Medsyn: Text-guided anatomy-aware synthesis of high-fidelity 3-d ct images. *IEEE Transactions on Medical Imaging* **43**(10), 3648–3660 (2024). <https://doi.org/10.1109/TMI.2024.3415032>
19. Yoon, J.S., Zhang, C., Suk, H.I., Guo, J., Li, X.: Sadm: Sequence-aware diffusion model for longitudinal medical image generation. In: *Information Processing in Medical Imaging* (2023). https://doi.org/10.1007/978-3-031-34048-2_30
20. Zhang, L., Rao, A., Agrawala, M.: Adding conditional control to text-to-image diffusion models (2023)